Integrated nanohole array surface plasmon resonance sensing device using a dual-wavelength source

2011 J. Micromech. Microeng. 21 115001

(http://iopscience.iop.org/0960-1317/21/11/115001)

J. Micromech. Microeng. **21** (2011) 115001 (6pp) doi:10.1088/0960-1317/21/11/115001

Integrated nanohole array surface plasmon resonance sensing device using a dual-wavelength source

C Escobedo[1], S Vincent[2], A I K Choudhury[2], J Campbell[2], A G Brolo[3], D Sinton[4] and R Gordon[2]

[1] Department of Mechanical Engineering, University of Victoria, PO Box 3055, STN CSC, V8W 3P6, Victoria, BC, Canada
[2] Department of Electrical and Computer Engineering, University of Victoria, PO Box 3055, V8W 3P6, Victoria, BC, Canada
[3] Department of Chemistry, University of Victoria, V8P 5C2, Victoria, BC, Canada
[4] Department of Mechanical and Industrial Engineering, University of Toronto, 5 King's College Rd, M5S 3G8, Toronto, ON, Canada

E-mail: gordon@uvic.ca and sinton@mie.utoronto.ca

Received 16 May 2011, in final form 23 August 2011
Published 3 October 2011
Online at stacks.iop.org/JMM/21/115001

Abstract
In this paper, we demonstrate a compact integrated nanohole array-based surface plasmon resonance sensing device. The unit includes a LED light source, driving circuitry, CCD detector, microfluidic network and computer interface, all assembled from readily available commercial components. A dual-wavelength LED scheme was implemented to increase spectral diversity and isolate intensity variations to be expected in the field. The prototype shows bulk sensitivity of 266 pixel intensity units/RIU and a limit of detection of 6×10^{-4} RIU. Surface binding tests were performed, demonstrating functionality as a surface-based sensing system. This work is particularly relevant for low-cost point-of-care applications, especially those involving multiple tests and field studies. While nanohole arrays have been applied to many sensing applications, and their suitability to device integration is well established, this is the first demonstration of a fully integrated nanohole array-based sensing device.

(Some figures in this article are in colour only in the electronic version)

1. Introduction

Common surface plasmon resonance (SPR) technologies currently used in biomedical applications rely on different coupling techniques including the Kretschmann configuration, and grating and waveguide couplers [1–3]. Specifically, the Kretschmann arrangement offers a high sensitivity, with a bulk detection limit on the order of 10^{-7} refractive index units or RIU [2, 3]. Assorted metal nanostructures that support surface plasmon excitations include nanoparticles [4] and nanoholes in metal films [5], the latter of which was found to exhibit extraordinary optical transmission (EOT) [6]. EOT resonances specifically depend on the refractive index near the surface, which has motivated the use of nanohole arrays as biosensors [7]. It was recognized early on that the collinear optical geometry of nanohole arrays is convenient for integration, further offering the potential for a high degree of multiplexing within a microfluidic environment [8]. The on-chip implementation of nanohole arrays involved a gold-on-glass substrate with arrays of nanoholes and a polydimethylsiloxane (PDMS) microfluidic layer reversibly bonded to the top [9]. The first nanohole array-based sensing demonstrations achieved smaller output sensitivities compared to the aforementioned Kretschmann configuration [10], and presently continue to be lower than the best Kretschmann sensors. Several approaches have been proposed in order to improve nanohole array-based SPR sensitivity, including devising analytical methodologies that increase the response to

binding events at the surface [11–15]. An example of this is the application of sandwich assays in SPR [16]. Furthermore, the fabrication of nanoholes generally involves nanofabrication methods, therefore introducing complexity and cost with respect to the Kretschmann SPR which requires a single thin metal film. However, these complexities have been reduced by advances in top-down methods (e.g., optical lithography [17, 18] and nanoimprint lithography [19]) and bottom-up methods (e.g., nanosphere lithography [20], and colloidal templating techniques [18, 21]). It has been shown that surface sensing from nanohole arrays produces up to 1192 nm RIU^{-1} shift in the EOT peak [3, 5, 7, 19–26].

An alternative to wavelength-shift detection in biosensing applications is to monitor the extent of adsorption by measuring the intensity variations from transmitted monochromatic beams [27, 28]. This has the benefit of simplifying the detection scheme (i.e. removing the need for a spectrometer), but reduces the spectral diversity of the detected signal. Consequently, the changes in light intensity used in this approach are often susceptible to spurious effects, such as drift in the sources or detectors and bulk matrix scattering as well as absorption [29]. In order to eliminate spurious effects associated with a single source at a particular wavelength, a second source at a different wavelength, responding in the opposite manner to the first source, may be added. In particular, if the intensity of the first source decreases to indicate a sensing event, this can be isolated from mere absorption or scattering of the light because the intensity of the second source should increase.

In this work, we demonstrate a hand-held integrated nanohole array-based sensing device with nine sensor elements, which is applicable to multiplexed detection [30]. This implementation is a significant step toward the use of SPR sensing technology for point-of-care and field testing applications. The device is based on nanohole array sensing, where the transmission spectrum of the nanohole array is modified by the local refractive index close to the metal surface. The device is tested through both bulk refractive index sensing and surface adsorption sensing experiments.

2. Experimental details

2.1. Overview of the integrated sensing platform

Figure 1 shows an image of the prototype device used in the experiments and schematic detailing the main components. A Videology 20K135USB board camera (generic industrial OEM CCD camera) with 1/4 inch format 720 × 480 pixel IL CCD and 8 bit ADC acted as the sensor array. LEDs with broad incoherent illumination as well as simple biasing circuitry were used as the light source. The LED was controlled by a driver circuit which in turn was controlled via MATLAB (Mathworks, MA). A chip assembly enclosed the substrate with the nanohole array sensors and a microfluidic chip responsible for interfacing the gold surface with selected test solutions. The nanohole array sensor was positioned at the center of the microfluidic channel with cross-sectional area of 100 μm by 70 μm, with a fluid volume of $\sim$ 7 pL

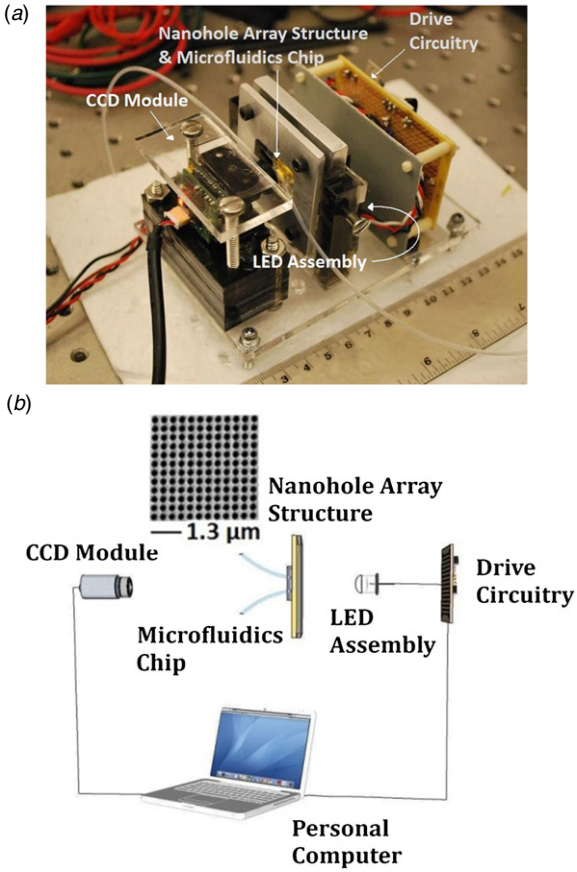

Figure 1. (*a*) Photograph of the SPR sensing device, with labels indicating components. (*b*) Schematic of the SPR imaging device, encompassing a standard experimental configuration for measuring light transmission through nine arrays of sub-wavelength holes. An SEM image of the nanohole array of 420 nm periodicity and 275 nm hole diameter is shown.

surrounding the sensor. Microfluidic solution delivery was achieved by means of a microscrew syringe pump (Harvard Apparatus, MA) via 1/16 inch outer diameter tubing (IDEX Health & Science LLC, Oak Harbor, WA). The chip assembly was clamped together using a customized metal frame with front and back openings for optical access and was mounted on a three-degrees-of-freedom positioning stage. Both the CCD camera and the circuitry containing the LEDs were positioned orthogonally with respect of the chip assembly as shown in figure 1(*b*). The CCD camera was configured to image the arrays directly by adjusting the lens provided. The light source control, as well as the image acquisition, was achieved by a separate computer via MATLAB. In order to partition the image into regions relevant to the individual nanohole arrays, nine 5 × 5 pixel grids were formed based on the location of the top-left pixel of each array's image. Signal responses for all nine nanohole arrays were simultaneously displayed in real time, since averaged pixel intensity (calculated through sampling 25 geometric points, whose result was temporally sampled at a rate of approximately 12 Hz) was displayed for both the red and green LEDs. The integrated sampling period was 10 s per LED wavelength. A metal housing (not illustrated) was utilized to reduce electromagnetic interference

and effect of external light signals. Details of the fabrication and assembly of the individual components of the device are provided next.

2.2. Nanofabrication of sub-wavelength hole arrays

The nanohole arrays were fabricated and imaged using a FEI dual-beam Strata 235 focused ion beam and a conventional scanning electron microscope. Device parameters such as the energy to which the gallium ions were accelerated, beam spot size, and the beam current were respectively set to 30 keV, 7.14 μm and 115 pA. A 3 × 3 array of sub-wavelength holes was milled into the 100 nm thick gold film on glass substrate (with a 1 nm chromium adhesion layer) commercially available from EMF. The array period was varied along the columns to be 420, 430 and 450 nm and the hole diameter was varied along the rows to be 225, 250 and 275 nm.

2.3. Microfluidic chip assembly

A PDMS chip was fabricated using a replica molding technique reported elsewhere [31, 32]. Using CAD software, a mask with a straight, 2 cm long microchannel measuring 200 μm in width and 70 μm in height was generated. A master of the microfluidic channel was fabricated by spin-coating SU-8 100 photoresist (MicroChem Corp., Newton, MA) onto a clean 7.62 cm silicon wafer (Silicon Quest International Inc., Santa Clara, CA), placing the mask over the coated wafer and exposing them to ultraviolet light for 84 s. The exposed wafer was post-baked for 10 min at 368 K and subsequently developed using SU-8 developer (MicroChem Corp., Newton, MA) Next, the master was hard baked at 338 K for 3 min and at 368 K for 22 min. A degassed, 13:1 mixture of Sylgard 184 elastomer (Dow Corning Corp., Midland, MI) and its curing agent was molded over the master. Upon baking the materials at 363 K for 25 min, the replica was removed from the mold. Holes for connecting Polyetheretherketone (PEEK) tubing (Upchurch Scientific, Oak Harbor, WA) were then punched at the microchannel ends for fluid entry. The microfluidic chip was finally aligned and sandwiched with the gold nanohole array substrate, all of which were encased by a 2.54 cm square metal frame with a large central opening for optical access.

3. Results and discussion

3.1. Two-color sensing

An initial microfluidic test was conducted to assess changes in refractive index using different solutions. One specific innovation of this device was the use of a dual-color LED. Figure 2(*a*) shows white light transmission through the nanohole arrays and LED spectra acquired using established SPR spectroscopy techniques [3, 7] prior to the microfluidic experiment. The degree of plasmon generation and the amount of transmitted light depend on several factors including the holes diameter, d, and pitch, p, and the dielectric constants of the metallic film and the surrounding medium, ε_{d} and ε_{m}, respectively. The approximate SPR wavelength can be defined

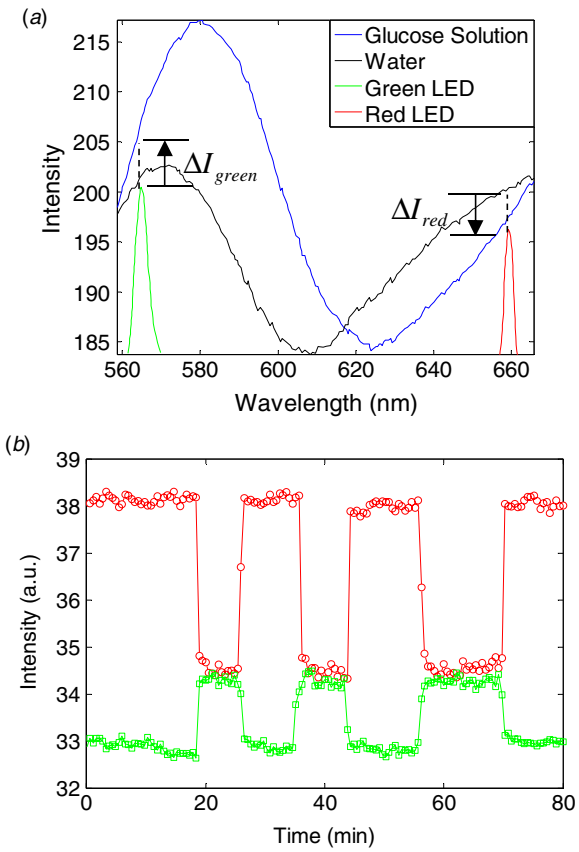

Figure 2. (*a*) Superimposed nanohole array and LED spectrums. (*b*) Proof-of-concept profile for alternating bulk refractive indices, $n_w = 1.3333$ and $n_\gamma = 1.3624$. Local minima for the output response of the red LED coupled with the maxima for that of the green relate to the event where the external dielectric has transitioned to the higher refractive index glucose solution.

by $\lambda(i, j) = p(i^2 + j^2)^{-1/2}(\varepsilon_d \varepsilon_m/(\varepsilon_d + \varepsilon_m))^{1/2}$, where i and j are related to the order of the grating [3, 29]. Figure 2(*a*) shows the transmission spectra at resonance wavelengths and the spectra from the red and green LEDs.

As shown in figure 2(*a*), the LED wavelengths were chosen such that one of them (green) increased its output intensity as the refractive index increased, and the other (red) decreased its output intensity. Thus, the LED's spectral maxima lies to the left and right of a nanohole array transmission peak (for a periodicity of 420 nm and diameter of 225 nm). Figure 2(*b*) shows the response of the nanohole arrays to the timed introduction of water and glucose solution at a flowrate on the order of ∼1 μl min^{-1}. A fast and repeatable sensor response to the change in refractive index in both red and green lines was found. The fast response is attributed to the small volume required to be replaced in the vicinity of the sensor of ∼ 7 pL. From 0 to 20 min at the start of the experiment, before the glucose is introduced, both the red and green line signals showed detectable, and repeatable, drift which was attributed to thermal effects. For that reason, a drift correction procedure was applied according to well-established methods [33]. Additionally, two aspects are noteworthy: (1) the magnitude of the signal change in response to the introduction of solutions with different indexes

of refraction is significantly higher than the drift, and (2) automated calibration before and after testing, as performed with commercial SPR units, would mitigate the influence of the drift on the measurement. The transmission coefficient was permitted to reach a steady-state value before reintroducing a liquid into the channel. The LED was toggled to temporally separate the green and red signals for detection on the CCD sensor. Compared to other works that used biaxial arrays [34] and multiple arrays of different periodicity [7, 9, 30], the two-color scheme benefits from allowing for uniform and uniaxial array fabrication, which is more amenable to low-cost fabrication methods.

3.2. Bulk sensitivity test

To determine the bulk sensitivity of the device, we prepared five test solutions of incremental concentrations (10%, 15%, 20%, 25% and 30%) of C_2H_5OH in H_2O. These solutions were then injected into the device in series. The combination of nanohole array and LED wavelength generating the largest shift in pixel intensity was found to be 250 nm diameter holes with 430 nm hole pitch and red LED. Figure 3(*a*) shows the step-waveform with the introduction of each subsequent solution of higher refractive index on this sensor (only red LED output is shown in this case). As shown, the system responded to each step change in refractive index. Perturbations in the signal in between solutions are attributed to the effect of solution mixing. Figure 3(*b*) plots the pixel intensity as a function of the bulk refractive index. From this figure, a sensitivity of 266 pixel intensity units/RIU was calculated. The dependent and independent variables are linearly related, with a squared Pearson's correlation coefficient of 0.989. The limit of detection (defined by signal-to-noise ratio of 3) was found to be 6×10^{-4} RIU. The applied statistical techniques are similar to the methods from a previous report by Hwang *et al* [35].

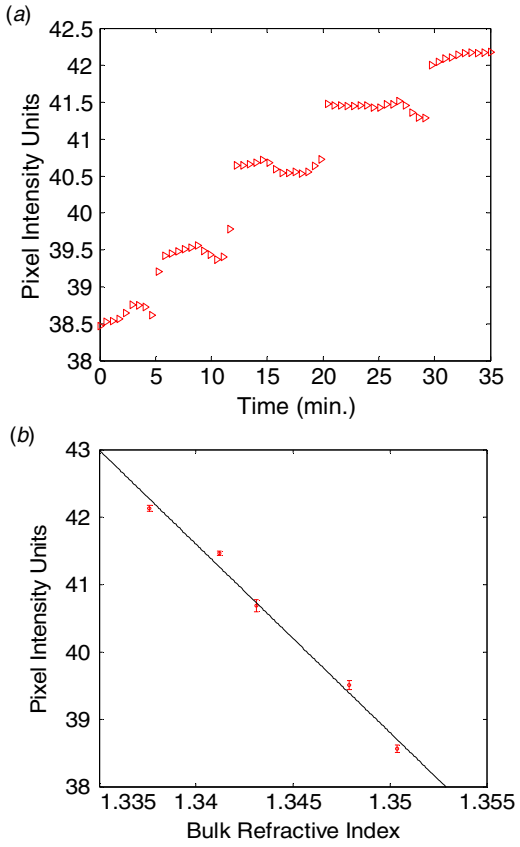

Figure 3. (*a*) Pixel intensity waveform for the array of 250 nm hole size and 430 nm hole pitch obtained through perturbing ethanol–water solution molarities. A moving average filter was applied to each step, where the fixed subset size was equal to three and zero-padded samples were discarded. (*b*) Line of best fit for a series of mean pixel intensities and bulk refractive index points, where the error bars represent the standard deviations for sample measurements.

3.3. Dynamic surface binding test

To demonstrate the sensor's ability to detect surface binding events, similar to processes used in quantitative biosensing, an analyte–receptor binding process was monitored [35, 36]. The biotin–streptavidin complex, with a dissociation constant on the order of $\sim 10^{-14}$ M, was selected for the experiment, given that it could reliably alter the surface refractive index [37]. Prior to the binding test, the nanohole array was plasma-cleaned for 15 min, sonicated in methanol for 5 min and immersed in a 5.18 mM cysteamine solution in water for 72 h to assemble a monolayer [9]. Upon completion of incubation it was then removed, gently rinsed with isopropyl alcohol as well as with purified water, and immersed in a 17.6 mM NHS–biotin solution in dimethyl sulfoxide (DMSO) for an additional 4 h. Following installation of the nanostructure into the chip assembly, preliminary volumes of pH 7 phosphate buffered saline (PBS) were flushed through the microchannels for a settling period of 20 min.

The experiment consisted of an initial 10 min PBS flush period followed by the subsequent introduction of the rest of the solutions. The signal was continuously acquired in order to assess the dynamic binding events at the nanohole arrays, as shown in figure 4. At 10 min, a 2 μM streptavidin solution in PBS was added. A gradual increase and decrease in transmission was observed for the red and the green source, respectively. At the 60 min mark, the sensor indicated that the surface concentration was saturated, and the system was flushed with PBS. The signal-to-noise ratio (SNR) of the curve was calculated by comparing it to the resultant signal from subtracting green and red LED output intensities as shown in figure 4(*b*). This was performed to establish that the SNR would increase, as the value rose from 11.4 (given $\mathrm{SNR_{Ori.}} = \mathrm{Signal_{Ori.}}/\mathrm{Noise_{Ori.}} = 0.570/0.0501 = 11.4$) for the original binding curve to 17.2 (given $\mathrm{SNR_{Sub.}} = \mathrm{Signal_{Sub.}}/\mathrm{Noise_{Sub.}} = 0.875/0.0510 = 17.2$) for the subtraction curve. As expected, the signal trend attained after the PBS flush was constant. This is related to the high affinity constant of the biotin–streptavidin system [38] in which the dissociation time is long (in the order of hours). It is also important to note that the long time for reaching saturation in this experiment might be due to the adsorption of the streptavidin to the inner tubing walls of the particular configuration used here, which may result in lower concentrations reaching the sensor at early times of the experiment. Another factor that may

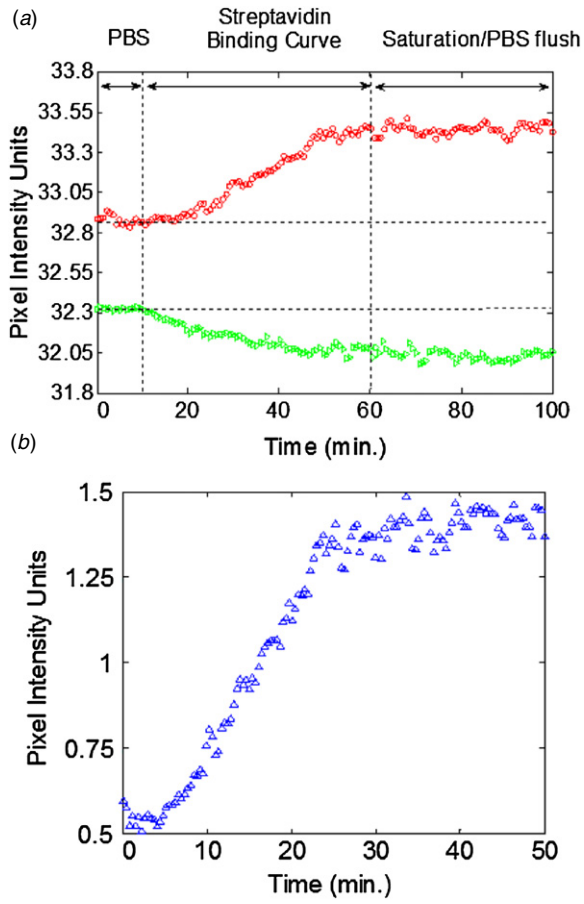

Figure 4. (*a*) Biotin–streptavidin binding curve for the array of 275 nm hole size and 420 nm hole pitch. The streptavidin solution was introduced at 10 min. And saturation was achieved after ∼40 min. (*b*) Plot of the difference between red and green LED pixel intensities, which enhances the SNR of the system. This can be seen by observing how the binding response has been magnified, having increased by an approximate factor of 1.51 (where $\mathrm{SNR_{Sub.}}/\mathrm{SNR_{Ori.}} = 17.2/11.4 = 1.51$).

play a role in the longer saturation time is the efficiency of the analyte collection at the sensing surface. The relative roles of cross-stream diffusion and advection on analyte collection efficiency has been discussed in recent studies [39, 40]. Most importantly, these results demonstrate that the integrated device enables the detection of surface binding. The device is also compatible with established methods to increase the transport of reactants to the nanohole array sensing surface, such as the flow-through nanohole array approach that we have shown to greatly increase the sensor response rate [39, 41].

4. Conclusions and outlook

In summary, we have developed an integrated, compact, nanohole array-based SPR sensing device. The device uses a two-color LED sensing scheme which can be used to distinguish between spurious sensing artifacts and the detection signal, as pairs of optical signals can be expected to exhibit complementary behavior. The result is a sensing system that would be immune to changes, for instance, in ambient light levels as expected in the field. Bulk sensing and dynamic surface binding were demonstrated, with a bulk sensitivity of 266 pixel intensity units/RIU, LOD of 6×10^{-4} RIU (with potential for improvement by two orders of magnitude), and sequential binding process response for 2 μM streptavidin to biotin. The integrated nature of this apparatus, as well as its relatively low component cost and potential for multiplexing, makes it a promising development for future point-of-care diagnostics and field research. Further optimization, by exploiting the full dynamic range of the sensor, can be expected to enable a three-fold improvement in LOD. Other improvements would come at the expense of increased complexity and cost, for example, by improving nanostructures which may exclude the use of broad-area, low cost lithographic fabrication of arrays. Importantly, this device is compatible with the flow-through nanohole array approach that has been shown to greatly increase sensor response rate and is specific to nanohole-based methods. In contrast, we do not believe that significant sensitivity enhancements can be achieved by increasing the number of nanoholes because the arrays already contain over 1100 nanoholes, which is well beyond the typical saturation in the spectral response of 300 nanoholes. Based on these factors, similar sensitivities to those reported recently for nanohole arrays [42], which lay in the order of 10^{-6} RIU, are anticipated with this configuration. However, alternative strategies can be adopted for increasing the sensitivity of the device, such as the introduction of adlayers on the gold surface of the nanohole arrays [43]. The results presented here indicate that it is feasible to exploit the various advantages of nanohole array-based sensing in a compact field-portable device.

Acknowledgments

CE would like to thank Chiara Valsecchi and Ryan Abel for their assistance and valuable discussions. This work was supported by the Canada Research Chairs program as well as the Natural Sciences and Engineering Research Council (NSERC) through a scholarship to CE, a research award to SV, Discovery Grants and the Strategic Network for Bioplasmonic Systems (Biopsys).

References

[1] Kretschmann E and Raether H 1968 Radiative decay of non-radiative surface plasmons excited by light *Z. Naturforsch.* A **23** 2135–6
[2] Byun K M 2010 Development of nanostructured plasmonic substrates for enhanced optical biosensing *J. Opt. Soc. Korea* **14** 65–76
[3] Homola J 2008 Surface plasmon resonance sensors for detection of chemical and biological species *Chem. Rev.* **108** 462–93
[4] Liu G L, Kim J, Lu Y and Lee P 2006 Optofluidic control using photothermal nanoparticles *Nature Mater.* **5** 27–32
[5] Gordon R, Sinton D, Kavanagh K L and Brolo A G 2008 A new generation of sensors based on extraordinary optical transmission *Acc. Chem. Res.* **41** 1049–57
[6] Ebbesen T W, Lezec H J, Ghaemi H F, Thio T and Wolff P A 1998 Extraordinary optical transmission through sub-wavelength hole arrays *Nature* **391** 667–9

[7] Brolo A G, Gordon R, Leathem B and Kavanagh K L 2004 Surface plasmon sensor based on the enhanced light transmission through arrays of nanoholes in gold films *Langmuir* **20** 4813–5

[8] Brolo A G, Ferreira J, Santos M J L, Escobedo C, Sinton D, Girotto E M, Eftekhari F and Gordon R 2008 Development of plasmonic substrates for biosensing *Proc. SPIE* **7035** 703503

[9] De Leebeeck A, Kumar L K S, de Lange V, Sinton D, Gordon R and Brolo A G 2007 On-chip surface-based detection with nanohole arrays *Anal. Chem.* **79** 4094–100

[10] Jung L S, Campbell C T, Chinowsky T M, Mar M N and Yee S S 1998 Quantitative interpretation of the response of surface plasmon resonance sensors to adsorbed films *Langmuir* **14** 5636–48

[11] Tetz K A, Pang L and Fainman Y 2006 High-resolution surface plasmon resonance sensor based on linewidth-optimized nanohole array transmittance *Opt. Lett.* **31** 1528–30

[12] Stark P R H, Halleck A E and Larson D N 2005 Short order nanohole arrays in metals for highly sensitive probing of local indices of refraction as the basis for a highly multiplexed biosensor technology *Methods* **37** 37–47

[13] Tetz K A, Rokitski R, Nezhad M and Fainman Y 2005 Excitation and direct imaging of surface plasmon polariton modes in a two-dimensional grating *Appl. Phys. Lett.* **86** 111110

[14] Lesuffleur A, Im H, Lindquist N C and Oh S-H 2007 Periodic nanohole arrays with shape-enhanced plasmon resonance as real-time biosensors *Appl. Phys. Lett.* **90** 243110

[15] Altewischer E, Genet C, van Exter M P, Woerdman J P, Alkemade P F A, Van Zuuk A and van der Drift E W J M 2005 Polarization tomography of metallic nanohole arrays *Opt. Lett.* **30** 90–2

[16] Homola J 2006 *Surface Plasmon Resonance Based Sensors* (Berlin: Springer)

[17] Menezes J W, Ferreira J, Santos M J L, Cescato L and Brolo A G 2010 Large-area fabrication of periodic arrays of nanoholes in metal films and their application in biosensing and plasmonic-enhanced photovoltaics *Adv. Funct. Mater.* **20** 918–24

[18] Pang L, Nakagawa W and Fainman Y 2003 Fabrication of two-dimensional photonic crystals with controlled defects by use of multiple exposures and direct-write *Appl. Opt.* **42** 5450–6

[19] Chou S Y, Krauss P R and Renstrom P J 1995 Imprint of sub-25 nm vias and trenches in polymers *Appl. Phys. Lett.* **67** 3114–6

[20] Haynes C L and Van Duyne R P 2001 Nanosphere lithography: a versatile nanofabrication tool for studies of size-dependent nanoparticle optics *J. Phys. Chem.* B **105** 5599–611

[21] Sun C-H, Min W-L and Jiang P 2008 Templated fabrication of sub-100 nm periodic nanostructures *Chem. Commun.* **27** 3163–5

[22] Liu Y and Blair S 2003 Fluorescence enhancement from an array of subwavelength metal apertures *Opt. Lett.* **28** 507–9

[23] Cooper M A 2003 Label-free screening of bio-molecular interactions *Anal. Bioanal. Chem.* **377** 834–42

[24] Li Y, Pan J, Zhan P, Zhu S, Ming N, Wang Z, Han W, Jiang X and Zi J 2010 Surface plasmon coupling enhanced dielectric environment sensitivity in a quasi-three-dimensional metallic nanohole array *Opt. Express* **18** 3546–55

[25] Jung L S, Campbell C T, Chinowsky T M, Mar M N and Yee S 1998 Quantitative interpretation of the response of surface plasmon resonance sensors to adsorbed films *Langmuir* **14** 5636–48

[26] Krishnan A, Thio T, Kim T J, Lezec H J, Ebbesen T W, Wolff P A, Pendry J, Martin-Moreno L and Garcia-Vidal F J 2001 Evanescently coupled resonance in surface plasmon enhanced transmission *Opt. Commun.* **200** 1–7

[27] Kim I T and Kihm K D 2006 Label-free visualization of microfluidic mixture concentration fields using a surface plasmon resonance (spr) reflectance imaging *Exp. Fluids* **41** 905-916

[28] Lesuffleur A, Im H, Lindquist N C, Lim K S and Oh S-H 2008 Laser-illuminated nanohole arrays for multiplex plasmonic microarray sensing *Opt. Express.* **16** 219–24

[29] Gordon R, Brolo A G, Sinton D and Kavanagh K L 2010 Resonant optical transmission through hole-arrays in metal films: physics and applications *Laser Photon. Rev.* **4** 311–35

[30] Lindquist N C, Lesuffleur A, Im H and Oh S-H 2009 Sub-micron resolution surface plasmon resonance imaging enabled by nanohole arrays with surrounding Bragg mirrors for enhanced sensitivity and isolation *Lab Chip* **9** 382–7

[31] Duffy D C, McDonald J C, Schueller J A and Whitesides G M 1998 Rapid prototyping of microfluidic systems in Poly(dimethylsiloxane) *Anal. Chem.* **70** 4974–84

[32] McDonald J C, Duffy D C, Anderson J R, Chiu D T, Wu H, Schueller O J A and Whitesides G M 2000 Fabrication of microfluidics systems in Poly(dimethylsiloxane) *Electrophoresis* **21** 27–40

[33] Salit M L and Turk G C 1998 A drift correction procedure *Anal. Chem.* **70** 3184–90

[34] Eftekhari F, Gordon R, Ferreira J, Brolo A G and Sinton D 2008 Polarization-dependent sensing of a self-assembled monolayer using biaxial nanohole arrays *Appl. Phys. Lett.* **92** 253103

[35] Hwang G M, Pang L, Mullen E H and Fainman Y 2008 Plasmonic sensing of biological analytes through nanoholes *IEEE Sens. J.* **8** 2074–9

[36] Pérez-Luna V H, O'Brien M J, Opperman K A, Hampton P D, López G P, Klumb L A and Stayton P S 1999 Molecular recognition between genetically engineered streptavidin and surface-bound biotin *J. Am. Chem. Soc.* **121** 6469–78

[37] Srisa-Art M, Dyson E C, deMello A J and Edel J B 2008 Monitoring of real-time streptavidin-biotin binding kinetics using droplet microfluidics *Anal. Chem.* **80** 7063–7

[38] Squires T M, Messinger R J and Manalis S R 2008 Making it stick: convection, reaction and diffusion in surface-based biosensors *Nature Biotechnol.* **26** 417–26

[39] Escobedo C, Brolo A G, Gordon R and Sinton D 2010 Flow-through versus flow-over: analysis of transport and binding in nanohole array plasmonic biosensors *Anal. Chem.* **82** 10015–20

[40] Ferreira J, Santos M J L, Rahman M M, Brolo A G, Gordon R, Sinton D and Girotto E M 2008 Attomolar protein detection using in-hole surface plasmon resonance *J. Am. Chem. Soc.* **131** 436–7

[41] Eftekhari F, Escobedo C, Ferreira J, Duan X, Girotto E M, Brolo A G, Gordon R and Sinton D 2009 Nanoholes as nanochannels: flow-through plasmonic sensing *Anal. Chem.* **81** 4308–11

[42] Lee K, Wu S and Wei P 2009 Intensity sensitivity of gold nanostructures and its application for high-throughput biosensing *Opt. Express* **17** 23104–13

[43] Skivesen N *et al* 2005 Optimization of metal-clad waveguide sensors *Sensors Actuators* B **106** 668–76